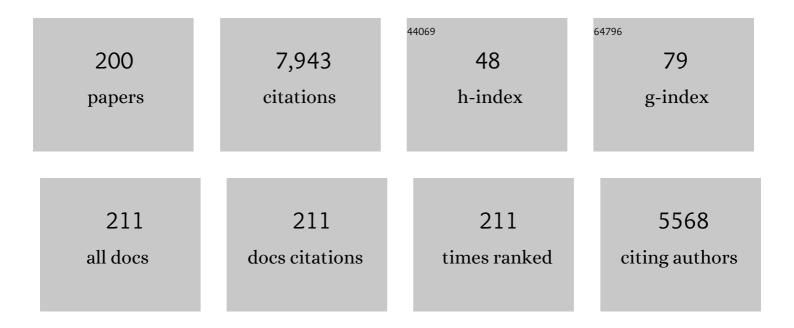
Qinhong Hu

List of Publications by Year in descending order

Source: https://exaly.com/author-pdf/4685124/publications.pdf Version: 2024-02-01



#	Article	IF	CITATIONS
1	Nano-scale pore structure and fractal dimension of organic-rich Wufeng-Longmaxi shale from Jiaoshiba area, Sichuan Basin: Investigations using FE-SEM, gas adsorption and helium pycnometry. Marine and Petroleum Geology, 2016, 70, 27-45.	3.3	431
2	Sources of anthropogenic radionuclides in the environment: a review. Journal of Environmental Radioactivity, 2010, 101, 426-437.	1.7	271
3	Accumulation of polycyclic aromatic hydrocarbons and heavy metals in lettuce grown in the soils contaminated with long-term wastewater irrigation. Journal of Hazardous Materials, 2008, 152, 506-515.	12.4	235
4	An Evaluation of Water Quality in Private Drinking Water Wells Near Natural Gas Extraction Sites in the Barnett Shale Formation. Environmental Science & Technology, 2013, 47, 10032-10040.	10.0	205
5	Low pore connectivity in natural rock. Journal of Contaminant Hydrology, 2012, 133, 76-83.	3.3	194
6	Nanoscale pore characteristics of the Lower Cambrian Niutitang Formation Shale: A case study from Well Yuke #1 in the Southeast of Chongqing, China. International Journal of Coal Geology, 2016, 154-155, 16-29.	5.0	164
7	Competitive adsorption of methane and ethane in montmorillonite nanopores of shale at supercritical conditions: A grand canonical Monte Carlo simulation study. Chemical Engineering Journal, 2019, 355, 76-90.	12.7	150
8	Soil to plant transfer of 238U, 226Ra and 232Th on a uranium mining-impacted soil from southeastern China. Journal of Environmental Radioactivity, 2005, 82, 223-236.	1.7	146
9	Estimating permeability using median pore-throat radius obtained from mercury intrusion porosimetry. Journal of Geophysics and Engineering, 2013, 10, 025014.	1.4	144
10	Sorption and transport of iodine species in sediments from the Savannah River and Hanford Sites. Journal of Contaminant Hydrology, 2005, 78, 185-205.	3.3	140
11	Low nanopore connectivity limits gas production in Barnett formation. Journal of Geophysical Research: Solid Earth, 2015, 120, 8073-8087.	3.4	135
12	Enhanced Transport of Low-Polarity Organic Compounds through Soil by Cyclodextrin. Environmental Science & Technology, 1994, 28, 952-956.	10.0	130
13	Pore characteristics of Longmaxi shale gas reservoir in the Northwest of Guizhou, China: Investigations using small-angle neutron scattering (SANS), helium pycnometry, and gas sorption isotherm. International Journal of Coal Geology, 2017, 171, 61-68.	5.0	124
14	Mineral types and organic matters of the Ordovician-Silurian Wufeng and Longmaxi Shale in the Sichuan Basin, China: Implications for pore systems, diagenetic pathways, and reservoir quality in fine-grained sedimentary rocks. Marine and Petroleum Geology, 2017, 86, 655-674.	3.3	118
15	Characterization of micro-nano pore networks in shale oil reservoirs of Paleogene Shahejie Formation in Dongying Sag of Bohai Bay Basin, East China. Petroleum Exploration and Development, 2017, 44, 720-730.	7.0	117
16	Supercritical Methane Diffusion in Shale Nanopores: Effects of Pressure, Mineral Types, and Moisture Content. Energy & Fuels, 2018, 32, 169-180.	5.1	115
17	Applying SANS technique to characterize nano-scale pore structure of Longmaxi shale, Sichuan Basin (China). Fuel, 2017, 197, 91-99.	6.4	113
18	Using X-ray computed tomography in pore structure characterization for a Berea sandstone: Resolution effect. Journal of Hydrology, 2012, 472-473, 254-261.	5.4	112

#	Article	IF	CITATIONS
19	Experimental investigations on the geometry and connectivity of pore space in organic-rich Wufeng and Longmaxi shales. Marine and Petroleum Geology, 2017, 84, 225-242.	3.3	107
20	Wettability of Mississippian Barnett Shale samples at different depths: Investigations from directional spontaneous imbibition. AAPG Bulletin, 2016, 100, 101-114.	1.5	103
21	Adsorption and desorption of iodine by various Chinese soils: II. Iodide and iodate. Geoderma, 2009, 153, 130-135.	5.1	102
22	Using flow interruption to identify factors causing nonideal contaminant transport. Journal of Contaminant Hydrology, 1997, 24, 205-219.	3.3	100
23	Pore structure characterization of organic-rich Niutitang shale from China: Small angle neutron scattering (SANS) study. International Journal of Coal Geology, 2018, 186, 115-125.	5.0	100
24	Pore characterization and methane sorption capacity of over-mature organic-rich Wufeng and Longmaxi shales in the southeast Sichuan Basin, China. Marine and Petroleum Geology, 2016, 77, 247-261.	3.3	99
25	Magnetic nanoscale Fe–Mn binary oxides loaded zeolite for arsenic removal from synthetic groundwater. Colloids and Surfaces A: Physicochemical and Engineering Aspects, 2014, 457, 220-227.	4.7	96
26	Pore connectivity and tracer migration of typical shales in south China. Fuel, 2017, 203, 32-46.	6.4	84
27	Aqueous-Phase Diffusion in Unsaturated Geologic Media: A Review. Critical Reviews in Environmental Science and Technology, 2003, 33, 275-297.	12.8	81
28	Effect of Solute Size on Transport in Structured Porous Media. Water Resources Research, 1995, 31, 1637-1646.	4.2	75
29	Using stable lead isotopes to trace heavy metal contamination sources in sediments of Xiangjiang and Lishui Rivers in China. Environmental Pollution, 2011, 159, 3406-3410.	7.5	75
30	Geochemical characteristics and origin of natural gas from Wufeng-Longmaxi shales of the Fuling gas field, Sichuan Basin (China). International Journal of Coal Geology, 2017, 171, 1-11.	5.0	75
31	Pore structure and spontaneous imbibition characteristics of marine and continental shales in China. AAPG Bulletin, 2018, 102, 1941-1961.	1.5	73
32	Initial water saturation and imbibition fluid affect spontaneous imbibition into Barnett shale samples. Journal of Natural Gas Science and Engineering, 2016, 34, 541-551.	4.4	72
33	A review of shale wettability characterization using spontaneous imbibition experiments. Marine and Petroleum Geology, 2019, 109, 330-338.	3.3	68
34	Pore structure, wettability, and spontaneous imbibition of Woodford Shale, Permian Basin, West Texas. Marine and Petroleum Geology, 2018, 91, 735-748.	3.3	65
35	Pore characterization of shales: A review of small angle scattering technique. Journal of Natural Gas Science and Engineering, 2020, 78, 103294.	4.4	64
36	Multiscale connectivity characterization of marine shales in southern China by fluid intrusion, small-angle neutron scattering (SANS), and FIB-SEM. Marine and Petroleum Geology, 2020, 112, 104101.	3.3	62

#	Article	IF	CITATIONS
37	Water adsorption characteristics of organic-rich Wufeng and Longmaxi Shales, Sichuan Basin (China). Journal of Petroleum Science and Engineering, 2020, 193, 107387.	4.2	61
38	Deposition of Platinum Nanoparticles, Synthesized in Water-in-Oil Microemulsions, on Alumina Supports. Langmuir, 2002, 18, 1811-1818.	3.5	59
39	Pore structure and tracer migration behavior of typical American and Chinese shales. Petroleum Science, 2015, 12, 651-663.	4.9	59
40	Organic nanopore structure and fractal characteristics of Wufeng and lower member of Longmaxi shales in southeastern Sichuan, China. Marine and Petroleum Geology, 2019, 103, 456-472.	3.3	59
41	Pore structure heterogeneity of Wufeng-Longmaxi shale, Sichuan Basin, China: Evidence from gas physisorption and multifractal geometries. Journal of Petroleum Science and Engineering, 2022, 208, 109313.	4.2	59
42	Laboratory measurement of water imbibition into low-permeability welded tuff. Journal of Hydrology, 2001, 242, 64-78.	5.4	58
43	Development of Geothermal Resources in China: A Review. Journal of Earth Science (Wuhan, China), 2018, 29, 452-467.	3.2	58
44	Effects of arsenic incorporation on jarosite dissolution rates and reaction products. Geochimica Et Cosmochimica Acta, 2013, 112, 192-207.	3.9	57
45	Wheat phytotoxicity from arsenic and cadmium separately and together in solution culture and in a calcareous soil. Journal of Hazardous Materials, 2007, 148, 377-382.	12.4	55
46	An NMR study of porous rock and biochar containing organic material. Microporous and Mesoporous Materials, 2013, 178, 94-98.	4.4	50
47	Integrated NMR and FE-SEM methods for pore structure characterization of Shahejie shale from the Dongying Depression, Bohai Bay Basin. Marine and Petroleum Geology, 2019, 100, 85-94.	3.3	50
48	Diffusivity of rocks: Gas diffusion measurements and correlation to porosity and pore size distribution. Water Resources Research, 2012, 48, .	4.2	49
49	Paleo-ocean redox environments of the Upper Ordovician Wufeng and the first member in lower Silurian Longmaxi formations in the Jiaoshiba area, Sichuan Basin. Canadian Journal of Earth Sciences, 2016, 53, 426-440.	1.3	48
50	Pore structure characteristics and permeability of deep sedimentary rocks determined by mercury intrusion porosimetry. Journal of Earth Science (Wuhan, China), 2016, 27, 670-676.	3.2	47
51	Applying Fractal Theory to Characterize the Pore Structure of Lacustrine Shale from the Zhanhua Depression in Bohai Bay Basin, Eastern China. Energy & Fuels, 2018, 32, 7539-7556.	5.1	47
52	Geological controls on the accumulation of shale gas: A case study of the early Cambrian shale in the Upper Yangtze area. Marine and Petroleum Geology, 2019, 107, 423-437.	3.3	45
53	Wettability and connectivity of overmature shales in the Fuling gas field, Sichuan Basin (China). AAPG Bulletin, 2019, 103, 653-689.	1.5	45
54	The effect of local-scale physical heterogeneity and nonlinear, rate-limited sorption/desorption on contaminant transport in porous media. Journal of Contaminant Hydrology, 2003, 64, 35-58.	3.3	44

#	Article	IF	CITATIONS
55	Integrating SANS and fluid-invasion methods to characterize pore structure of typical American shale oil reservoirs. Scientific Reports, 2017, 7, 15413.	3.3	44
56	Pore structure, wettability and tracer migration in four leading shale formations in the Middle Yangtze Platform, China. Marine and Petroleum Geology, 2018, 89, 415-427.	3.3	44
57	Mineral composition and seal condition implicated in pore structure development of organic-rich Longmaxi shales, Sichuan Basin, China. Marine and Petroleum Geology, 2018, 98, 507-522.	3.3	44
58	Mobility of arsenic in aquifer sediments at Datong Basin, northern China: Effect of bicarbonate and phosphate. Journal of Geochemical Exploration, 2013, 135, 93-103.	3.2	43
59	Nuclear magnetic resonance T2 spectrum: multifractal characteristics and pore structure evaluation. Applied Geophysics, 2017, 14, 205-215.	0.6	42
60	The effects of mineral composition, TOC content and pore structure on spontaneous imbibition in Lower Jurassic Dongyuemiao shale reservoirs. Marine and Petroleum Geology, 2019, 109, 268-278.	3.3	42
61	Lead adsorption by biochar under the elevated competition of cadmium and aluminum. Scientific Reports, 2017, 7, 2264.	3.3	41
62	Experimental investigation of water vapor adsorption isotherm on gas-producing Longmaxi shale: Mathematical modeling and implication for water distribution in shale reservoirs. Chemical Engineering Journal, 2021, 406, 125982.	12.7	41
63	Effect of shale diagenesis on pores and storage capacity in the Paleogene Shahejie Formation, Dongying Depression, Bohai Bay Basin, east China. Marine and Petroleum Geology, 2019, 103, 738-752.	3.3	39
64	Sensitive parameters of NMR T2 spectrum and their application to pore structure characterization and evaluation in logging profile: A case study from Chang 7 in the Yanchang Formation, Heshui area, Ordos Basin, NW China. Marine and Petroleum Geology, 2020, 111, 230-239.	3.3	39
65	Rock fabric and pore structure of the Shahejie sandy conglomerates from the Dongying depression in the Bohai Bay Basin, East China. Marine and Petroleum Geology, 2018, 97, 624-638.	3.3	38
66	Quartz types, silica sources and their implications for porosity evolution and rock mechanics in the Paleozoic Longmaxi Formation shale, Sichuan Basin. Marine and Petroleum Geology, 2021, 128, 105036.	3.3	38
67	Quantitative 3-D Elemental Mapping by LA-ICP-MS of a Basaltic Clast from the Hanford 300 Area, Washington, USA. Environmental Science & Technology, 2012, 46, 2025-2032.	10.0	36
68	Geochemical characteristics of the Silurian shales from the central Taurides, southern Turkey: Organic matter accumulation, preservation and depositional environment modeling. Marine and Petroleum Geology, 2019, 102, 155-175.	3.3	36
69	Nanoscale Pore Network Evolution of Xiamaling Marine Shale during Organic Matter Maturation by Hydrous Pyrolysis. Energy & Fuels, 2020, 34, 1548-1563.	5.1	36
70	Effect of reducing groundwater on the retardation of redox-sensitive radionuclides. Geochemical Transactions, 2008, 9, 12.	0.7	34
71	Sorption, degradation, and transport of methyl iodide and other iodine species in geologic media. Applied Geochemistry, 2012, 27, 774-781.	3.0	34
72	A unified model for the formation and distribution of both conventional and unconventional hydrocarbon reservoirs. Geoscience Frontiers, 2021, 12, 695-711.	8.4	34

#	Article	IF	CITATIONS
73	Biodegradation during Contaminant Transport in Porous Media. 2. The Influence of Physicochemical Factors. Environmental Science & Technology, 1999, 33, 96-103.	10.0	33
74	Effects of anion competitive adsorption on arsenic enrichment in groundwater. Journal of Environmental Science and Health - Part A Toxic/Hazardous Substances and Environmental Engineering, 2011, 46, 471-479.	1.7	33
75	Laminae characteristics and influence on shale gas reservoir quality of lower Silurian Longmaxi Formation in the Jiaoshiba area of the Sichuan Basin, China. Marine and Petroleum Geology, 2019, 109, 839-851.	3.3	33
76	Fluoride and arsenic hydrogeochemistry of groundwater at Yuncheng basin, Northern China. Geochemistry International, 2014, 52, 868-881.	0.7	32
77	Pressure–dependent fracture permeability of marine shales in the Northeast Yunnan area, Southern China. International Journal of Coal Geology, 2019, 214, 103237.	5.0	31
78	Pore connectivity and water accessibility in Upper Permian transitional shales, southern China. Marine and Petroleum Geology, 2019, 107, 407-422.	3.3	31
79	Particle size effect on water vapor sorption measurement of organic shale: One example from Dongyuemiao Member of Lower Jurassic Ziliujing Formation in Jiannan Area of China. Advances in Geo-Energy Research, 2020, 4, 207-218.	6.0	31
80	Quantitative structureâ€activity relationships for evaluating the influence of sorbate structure on sorption of organic compounds by soil. Environmental Toxicology and Chemistry, 1995, 14, 1133-1140.	4.3	30
81	Transport of rate-limited sorbing solutes in an aggregated porous medium: A multiprocess non-ideality approach. Journal of Contaminant Hydrology, 1996, 24, 53-73.	3.3	30
82	Scale dependence of intragranular porosity, tortuosity, and diffusivity. Water Resources Research, 2010, 46, .	4.2	30
83	Competitive adsorption of humic acid and arsenate on nanoscale iron–manganese binary oxide-loaded zeolite in groundwater. Journal of Geochemical Exploration, 2014, 144, 220-225.	3.2	30
84	Spontaneous Imbibition of Three Leading Shale Formations in the Middle Yangtze Platform, South China. Energy & Fuels, 2017, 31, 6903-6916.	5.1	30
85	Complementary neutron scattering, mercury intrusion and SEM imaging approaches to micro- and nano-pore structure characterization of tight rocks: A case study of the Bakken shale. International Journal of Coal Geology, 2019, 212, 103252.	5.0	30
86	The effect of clay-swelling induced cracks on imbibition behavior of marine shale reservoirs. Journal of Natural Gas Science and Engineering, 2020, 83, 103525.	4.4	30
87	Preliminary 3-D site-scale studies of radioactive colloid transport in the unsaturated zone at Yucca Mountain, Nevada. Journal of Contaminant Hydrology, 2003, 60, 251-286.	3.3	29
88	Main controls and geological sweet spot types in Paleogene shale oil rich areas of the Jiyang Depression, Bohai Bay basin, China. Marine and Petroleum Geology, 2020, 111, 576-587.	3.3	29
89	The effect of solute size on diffusive-dispersive transport in porous media. Journal of Hydrology, 1994, 158, 305-317.	5.4	28
90	Coupled effects of nonlinear, rateâ€limited sorption and biodegradation on transport of 2,4â€dichlorophenoxyacetic acid in soil. Environmental Toxicology and Chemistry, 1998, 17, 1673-1680.	4.3	28

#	Article	IF	CITATIONS
91	Characterizing Unsaturated Diffusion in Porous Tuff Gravel. Vadose Zone Journal, 2004, 3, 1425-1438.	2.2	27
92	Mineral-controlled nm-μm-scale pore structure of saline lacustrine shale in Qianjiang Depression, Jianghan Basin, China. Marine and Petroleum Geology, 2019, 99, 347-354.	3.3	27
93	A new and integrated imaging and compositional method to investigate the contributions of organic matter and inorganic minerals to the pore spaces of lacustrine shale in China. Marine and Petroleum Geology, 2021, 127, 104962.	3.3	27
94	Assessing field-scale migration of radionuclides at the Nevada Test Site: "mobile―species. Journal of Environmental Radioactivity, 2008, 99, 1617-1630.	1.7	26
95	Developmental characteristics and controlling factors of natural fractures in the lower paleozoic marine shales of the upper Yangtze Platform, southern China. Journal of Natural Gas Science and Engineering, 2020, 76, 103191.	4.4	26
96	Pore structure typing and fractal characteristics of lacustrine shale from Kongdian Formation in East China. Journal of Natural Gas Science and Engineering, 2021, 85, 103709.	4.4	26
97	Origin of over-pressure in clastic rocks in Yuanba area, northeast Sichuan Basin, China. Journal of Natural Gas Science and Engineering, 2016, 30, 90-105.	4.4	23
98	Fluid distribution and gas adsorption behaviors in over-mature shales in southern China. Marine and Petroleum Geology, 2019, 109, 223-232.	3.3	23
99	Diagenesis and pore evolution for various lithofacies of the Wufeng-Longmaxi shale, southern Sichuan Basin, China. Marine and Petroleum Geology, 2021, 133, 105251.	3.3	23
100	Applying Molecular and Nanoparticle Tracers to Study Wettability and Connectivity of Longmaxi Formation in Southern China. Journal of Nanoscience and Nanotechnology, 2017, 17, 6284-6295.	0.9	22
101	Pore connectivity characterization of shale using integrated wood's metal impregnation, microscopy, tomography, tracer mapping and porosimetry. Fuel, 2020, 259, 116248.	6.4	22
102	Factors controlling organic-matter accumulation in the Upper Ordovician-Lower Silurian organic-rich shale on the northeast margin of the Upper Yangtze platform: Evidence from petrographic and geochemical proxies. Marine and Petroleum Geology, 2020, 121, 104597.	3.3	22
103	A statistical method to detect ordering and phase separation by APFIM. Ultramicroscopy, 1998, 73, 279-285.	1.9	21
104	Comparative Investigations on Wettability of Typical Marine, Continental, and Transitional Shales in the Middle Yangtze Platform (China). Energy & Fuels, 2018, 32, 12187-12197.	5.1	21
105	Characterization of Closed Pores in Longmaxi Shale by Synchrotron Small-Angle X-ray Scattering. Energy & Fuels, 2021, 35, 6738-6754.	5.1	21
106	Non-connected pores of the Longmaxi shale in southern Sichuan Basin of China. Marine and Petroleum Geology, 2019, 110, 420-433.	3.3	20
107	Microfracture-pore structure characterization and water-rock interaction in three lithofacies of the Lower Eagle Ford Formation. Engineering Geology, 2021, 292, 106276.	6.3	20
108	Simultaneous analyses and applications of multiple fluorobenzoate and halide tracers in hydrologic studies. Hydrological Processes, 2005, 19, 2671-2687.	2.6	19

#	Article	IF	CITATIONS
109	Field tracer-transport tests in unsaturated fractured tuff. Journal of Contaminant Hydrology, 2001, 51, 1-12.	3.3	18
110	Solvent extraction efficiency of an Eocene-aged organic-rich lacustrine shale. Marine and Petroleum Geology, 2021, 126, 104941.	3.3	18
111	Microscopic pore-fracture configuration and gas-filled mechanism of shale reservoirs in the western Chongqing area, Sichuan Basin, China. Petroleum Exploration and Development, 2021, 48, 1063-1076.	7.0	18
112	Tracer Penetration into Welded Tuff Matrix from Flowing Fractures. Vadose Zone Journal, 2002, 1, 102-112.	2.2	17
113	Effects of Fe-rich acid mine drainage on percolation features and pore structure in carbonate rocks. Journal of Hydrology, 2020, 591, 125571.	5.4	17
114	Thermal maturity evaluation using Raman spectroscopy for oil shale samples of USA: comparisons with vitrinite reflectance and pyrolysis methods. Petroleum Science, 2020, 17, 567-581.	4.9	17
115	ARSENATE TOXICITY FOR WHEAT AND LETTUCE IN SIX CHINESE SOILS WITH DIFFERENT PROPERTIES. Environmental Toxicology and Chemistry, 2009, 28, 1946.	4.3	16
116	KG²B, a collaborative benchmarking exercise for estimating the permeability of the Grimsel granodiorite – Part 1: measurements, pressure dependence and pore-fluid effects. Geophysical Journal International, 2018, 215, 799-824.	2.4	16
117	Clarifying pore diameter, pore width, and their relationship through pressure measurements: A critical study. Marine and Petroleum Geology, 2019, 107, 142-148.	3.3	16
118	Spatial heterogeneity analyses of pore structure and mineral composition of Barnett Shale using X-ray scattering techniques. Marine and Petroleum Geology, 2021, 134, 105354.	3.3	16
119	The effects of pore structure on wettability and methane adsorption capability of Longmaxi Formation shale from the southern Sichuan Basin in China. AAPG Bulletin, 2020, 104, 1375-1399.	1.5	15
120	Characterization of methane adsorption on shale of a complex tectonic area in Northeast Guizhou, China: Experimental results and geological significance. Journal of Natural Gas Science and Engineering, 2020, 84, 103676.	4.4	15
121	Pore Geometry Characteristics and Fluid–Rock Interaction in the Haynesville Shale, East Texas, United States. Energy & Fuels, 2021, 35, 237-250.	5.1	15
122	GAS DIFFUSIVITY IN POROUS MEDIA: DETERMINATION BY MERCURY INTRUSION POROSIMETRY AND CORRELATION TO POROSITY AND PERMEABILITY. Journal of Porous Media, 2013, 16, 607-617.	1.9	15
123	Characterizing the contribution of diffusive mass transfer to solute transport in sedimentary aquifer systems at laboratory and field scales. Journal of Hydrology, 2003, 276, 275-286.	5.4	14
124	Unsaturated flow and transport through a fault embedded in fractured welded tuff. Water Resources Research, 2004, 40, .	4.2	14
125	Contamination investigation and risk assessment of molybdenum on an industrial site in China. Journal of Geochemical Exploration, 2014, 144, 273-281.	3.2	14
126	Coupled nano-petrophysical and organic-geochemical study of the Wolfberry Play in Howard County, Texas U.S.A Marine and Petroleum Geology, 2020, 122, 104663.	3.3	14

#	Article	IF	CITATIONS
127	Fracture characteristics and logging identification of lacustrine shale in the Jiyang Depression, Bohai Bay Basin, Eastern China. Marine and Petroleum Geology, 2021, 132, 105192.	3.3	14
128	Application of Laser Ablation-Inductively Coupled Plasma-Mass Spectrometry to studies of chemical diffusion, sorption, and transport in natural rock. Geochemical Journal, 2012, 46, 459-475.	1.0	13
129	Evolution of Shale Microstructure under in Situ Heat Treatment: Synchrotron Small-Angle X-ray Scattering. Energy & Fuels, 2021, 35, 4345-4357.	5.1	13
130	Petrophysical Characteristics of Silurian Mudstones from Central Taurides in Southern Turkey. Journal of Earth Science (Wuhan, China), 2021, 32, 778-798.	3.2	13
131	INVESTIGATING THE EFFECT OF MEDIAN PORE-THROAT DIAMETER ON SPONTANEOUS IMBIBITION. Journal of Porous Media, 2015, 18, 1231-1238.	1.9	13
132	Distribution of 99Tc and 129I in the vicinity of underground nuclear tests at the Nevada Test Site. Journal of Radioanalytical and Nuclear Chemistry, 2008, 276, 755-761.	1.5	12
133	Geochemical Cycling of Iodine Species in Soils. , 2009, , 93-105.		12
134	Uranium release from different size fractions of sediments in Hanford 300 area, Washington, USA. Journal of Environmental Radioactivity, 2012, 107, 92-94.	1.7	12
135	Fractionation and speciation of arsenic in fresh and combusted coal wastes from Yangquan, northern China. Environmental Geochemistry and Health, 2012, 34, 113-122.	3.4	12
136	Quantifying Fluidâ€Wettable Effective Pore Space in the Utica and Bakken Oil Shale Formations. Geophysical Research Letters, 2020, 47, e2020GL087896.	4.0	12
137	Radionuclide transport in fractured granite interface zones. Physics and Chemistry of the Earth, 2008, 33, 1042-1049.	2.9	11
138	Modeling intragranular diffusion in lowâ€connectivity granular media. Water Resources Research, 2012, 48, .	4.2	11
139	Grain-Size Based Additivity Models for Scaling Multi-rate Uranyl Surface Complexation in Subsurface Sediments. Mathematical Geosciences, 2016, 48, 511-535.	2.4	11
140	Effect of Particle Size on Pore Characteristics of Organic-Rich Shales: Investigations from Small-Angle Neutron Scattering (SANS) and Fluid Intrusion Techniques. Energies, 2020, 13, 6049.	3.1	11
141	Fracturing flowback fluids from shale gas wells in western chongqing: Geochemical analyses and relevance for exploration & development. Journal of Natural Gas Science and Engineering, 2021, 88, 103821.	4.4	11
142	Pore Accessibility and Connectivity of Mineral and Kerogen Phases for Shales. , 2014, , .		10
143	USING MULTICYCLE MERCURY INTRUSION POROSIMETRY TO INVESTIGATE HYSTERESIS PHENOMENON OF DIFFERENT POROUS MEDIA. Journal of Porous Media, 2018, 21, 607-622.	1.9	10
144	KG²B, a collaborative benchmarking exercise for estimating the permeability of the Grimsel granodiorite—Part 2: modelling, microstructures and complementary data. Geophysical Journal International, 2018, 215, 825-843.	2.4	10

#	Article	IF	CITATIONS
145	Investigation of Microwave Irradiation Stimulation to Enhance the Pore Connectivity of Shale. Energy & Fuels, 2021, 35, 3240-3251.	5.1	10
146	Porosity measurement of granular rock samples by modified bulk density analyses with particle envelopment. Marine and Petroleum Geology, 2021, 133, 105273.	3.3	10
147	Hydrocarbon accumulation depth limit and implications for potential resources prediction. Gondwana Research, 2022, 103, 389-400.	6.0	10
148	Pore accessibility by wettable fluids in overmature marine shales of China: Investigations from contrast-matching small-angle neutron scattering (CM-SANS). International Journal of Coal Geology, 2022, 255, 103987.	5.0	10
149	Anthropogenic impact assessment of Niangziguan karst water. Water Management, 2011, 164, 495-510.	1.2	9
150	Assessing Molybdenum Adsorption onto an Industrial Soil and Iron Minerals. Water, Air, and Soil Pollution, 2013, 224, 1.	2.4	9
151	Pore structure and fluid saturation of near-oil source low-permeability turbidite sandstone of the Dongying Sag in the Bohai Bay Basin, east China. Journal of Petroleum Science and Engineering, 2021, 196, 108106.	4.2	9
152	Porosity and Pore Networks in Tight Dolostone—Mudstone Reservoirs: Insights from the Devonian Three Forks Formation, Williston Basin, USA. Journal of Earth Science (Wuhan, China), 2022, 33, 462-481.	3.2	9
153	Biodegradation during contaminant transport in porous media: 3. Apparent condition-dependency of growth-related coefficients. Journal of Contaminant Hydrology, 2001, 50, 209-223.	3.3	8
154	Leaching behavior of trace elements in coal spoils from Yangquan coal mine, Northern China. Journal of Earth Science (Wuhan, China), 2016, 27, 891-900.	3.2	8
155	Ceological controls and methane sorption capacity of marine shales of the Fuling shale gas field in the eastern Sichuan Basin, China. Petroleum Geoscience, 2017, 23, 466-475.	1.5	8
156	Lower Es3 in Zhanhua Sag, Jiyang Depression: a case study for lithofacies classification in lacustrine mud shale. Applied Geophysics, 2018, 15, 151-164.	0.6	8
157	Origin of authigenic quartz in organic-rich shales of the Niutitang Formation in the northern margin of Sichuan Basin, South China: Implications for pore network development. Marine and Petroleum Geology, 2022, 138, 105548.	3.3	8
158	Sorption of strontium and fractal scaling of the heterogeneous media in a candidate VLLW disposal site. Journal of Radioanalytical and Nuclear Chemistry, 2010, 283, 319-328.	1.5	7
159	Conversion, sorption, and transport of arsenic species in geological media. Applied Geochemistry, 2012, 27, 2197-2203.	3.0	7
160	Changes in water vapor adsorption and water film thickness in clayey materials as a function of relative humidity. Vadose Zone Journal, 2020, 19, e20063.	2.2	7
161	Effect of Shale Sample Particle Size on Pore Structure Obtained from High Pressure Mercury Intrusion Porosimetry. Geofluids, 2021, 2021, 1-15.	0.7	7
162	Impacts of pH-dependent metal speciation on the decomposition of triclosan by sulfate radicals. Water Science and Technology: Water Supply, 2012, 12, 837-843.	2.1	6

#	Article	IF	CITATIONS
163	Nanopetrophysical characterization of the Mancos Shale Formation in the San Juan Basin of northwestern New Mexico, USA. Interpretation, 2019, 7, SJ45-SJ65.	1.1	6
164	Multiple Approaches to Quantifying the Effective Porosity of Lacustrine Shale Oil Reservoirs in Bohai Bay Basin, East China. Geofluids, 2020, 2020, 1-13.	0.7	6
165	Pore Structure Characterization and Reservoir Quality Evaluation of Analcite-Rich Shale Oil Reservoir from the Bohai Bay Basin. Energy & Fuels, 2021, 35, 9349-9368.	5.1	6
166	Geochemical, petrographic and reservoir characteristics of the transgressive systems tract of lower Silurian black shale in Jiaoshiba area, southwest China. Marine and Petroleum Geology, 2021, 129, 105014.	3.3	6
167	Development of an NMR workflow for determining nano-petrophysical properties of marine and lacustrine mudrocks. Journal of Petroleum Science and Engineering, 2022, 214, 110491.	4.2	6
168	Characterizing Unsaturated Diffusion in Porous Tuff Gravel. Vadose Zone Journal, 2004, 3, 1425-1438.	2.2	5
169	Detection of tritium sorption on four soil materials. Journal of Environmental Radioactivity, 2011, 102, 212-216.	1.7	5
170	USING SPONTANEOUS WATER IMBIBITION TO MEASURE THE EFFECTIVE PERMEABILITY OF BUILDING MATERIALS. Special Topics and Reviews in Porous Media, 2012, 3, 209-213.	1.1	5
171	Pore Structure and Fluid Uptake of the Springer/Goddard Shale Formation in Southeastern Oklahoma, USA. Geofluids, 2018, 2018, 1-16.	0.7	5
172	Resolution effect on image-based conventional and tight sandstone pore space reconstructions: Origins and strategies. Journal of Hydrology, 2020, 586, 124856.	5.4	5
173	Recent advances in the mechanical characterization of shales at nano-to micro-scales: A review. Mechanics of Materials, 2021, 162, 104043.	3.2	5
174	Chemical Structure Transformations in Kerogen from Longmaxi Shales in Response to Tectonic Stress as Investigated by HRTEM, FTIR, and ¹³ C NMR. Energy & Fuels, 2021, 35, 19496-19506.	5.1	5
175	Recharge processes and groundwater evolution of multiple aquifers, Beijing, China. Water Management, 2012, 165, 411-424.	1.2	4
176	Adsorption Mechanism of Humic Acid on Cu/Fe Bimetallic Particles and Its Influence on the Reduction of Nitrobenzene in Groundwater. Water, Air, and Soil Pollution, 2014, 225, 1.	2.4	4
177	Roles of aqueous Fe(III) in oxidation of partially reduced nontronite under sub-acidic conditions. Applied Clay Science, 2020, 195, 105689.	5.2	4
178	Tracer Penetration into Welded Tuff Matrix from Flowing Fractures. Vadose Zone Journal, 2002, 1, 102-112.	2.2	4
179	Tracer Penetration into Welded Tuff Matrix from Flowing Fractures. Vadose Zone Journal, 2002, 1, 102.	2.2	4
180	Water Saturation and Distribution Variation in Coal Reservoirs: Intrusion and Drainage Experiments Using One- and Two-Dimensional NMR Techniques. Energy & Fuels, 2022, 36, 6130-6143.	5.1	4

#	Article	IF	CITATIONS
181	Field-Scale Migration of ⁹⁹ Tc and ¹²⁹ I at the Nevada Test Site. Materials Research Society Symposia Proceedings, 2004, 824, 336.	0.1	3
182	Factors influencing plutonium sorption in shale media. Radiochimica Acta, 2010, 98, .	1.2	3
183	LA-ICP-MS Calibrations for Intact Rock Samples with Internal Standard and Modified Constant-Sum Methods. American Journal of Analytical Chemistry, 2012, 03, 168-174.	0.9	3
184	Pore structure and fluid uptake of the Yeso, Abo, and Cisco Formations in the Permian Basin in southeast New Mexico, USA. Interpretation, 2019, 7, SK1-SK17.	1.1	3
185	An improved liquid-liquid extraction technique to determine shale wettability. Marine and Petroleum Geology, 2022, 138, 105538.	3.3	3
186	Comment on "Effect of solute size on transport in structured porous media―by Qinhong Hu and Mark L. Brusseau. Water Resources Research, 1997, 33, 359-361.	4.2	2
187	Experimental Validation of Retardation of Tritium Migration in the Chinese Loess Media. Water, Air, and Soil Pollution, 2011, 215, 497-506.	2.4	2
188	Effects of Confining Pressure on Unsteady‣tate Air Permeability Measurement Method in an Aggregated Andisol. Vadose Zone Journal, 2016, 15, 1-9.	2.2	2
189	Pore Structure, Wettability, and Their Coupled Effects on Tracer-Containing Fluid Migration in Organic-Rich Shale. , 2019, , 133-154.		2
190	Micro- and Nanoscale Pore Structure Characterization of Carbonates from the Xiaoerbulake Formation in the Tarim Basin, Northwest China. Geofluids, 2021, 2021, 1-20.	0.7	2
191	Tracer migration experiments in unsaturated fractured tuff. Geochemical Journal, 2004, 38, 177-189.	1.0	1
192	A New Model for Simulating the Imbibition of a Wetting-Phase Fluid in a Matrix-Fracture Dual Connectivity System. Geofluids, 2022, 2022, 1-18.	0.7	1
193	Analyses of True-Triaxial Hydraulic Fracturing of Granite Samples for an Enhanced Geothermal System. Lithosphere, 2022, 2021, .	1.4	1
194	Quantitative Characterization of Full-Spectrum Pore Size and Connectivity for Shale with Different Sedimentary Facies from the Dongying Depression, Bohai Bay Basin, East China. Geofluids, 2022, 2022, 1-17.	0.7	1
195	Dispersive—diffusive transport of non-sorbed solute in multicomponent solutions. Journal of Contaminant Hydrology, 1995, 19, 261-267.	3.3	0
196	Reply [to "Comment on â€~Effect of solute size on transport in structured porous media' by Qinhong Hu and Mark L. Brusseauâ€]. Water Resources Research, 1997, 33, 363-366.	4.2	0
197	Fate and transport of radionuclides in the environment: A dedicated symposium within the 9th International Conference on Biogeochemistry of Trace Elements, Beijing (2007). Journal of Environmental Radioactivity, 2010, 101, 425.	1.7	0
198	Construction of Normal Compaction Trends for Overpressure Prediction in Organic-rich Shales. , 2016, , .		0

#	Article	IF	CITATIONS
199	Optimization of Brittleness Estimation Using Rock Physics Templates. , 2017, , .		0
200	A Workflow for Target-oriented Pore Pressure Prediction in Shale Gas Reservoirs. , 2017, , .		0